ACADEMIC PRESS

Available online at www.sciencedirect.com
SCIENCE DIRECT®

Journal of Catalysis 216 (2003) 63–72

JOURNAL OF CATALYSIS

www.elsevier.com/locate/jcat

Kinetic interpretation of catalytic activity patterns based on theoretical chemical descriptors

Hervé Toulhoat [a,*] and Pascal Raybaud [b]

[a] *Direction Scientifique, Institut Français du Pétrole, 1 & 4 avenue de Bois-Préau, 92832, Rueil-Malmaison cedex, France*
[b] *Division Chimie et Physico-Chimie Appliquées, Institut Français du Pétrole, 1 & 4 avenue de Bois-Préau, 92832, Rueil-Malmaison cedex, France*

Received 8 July 2002; revised 24 October 2002; accepted 4 November 2002

Abstract

We introduce descriptors of bond energies, calculated at the DFT level for bulk crystalline structures. We show the relevance of these descriptors for surface bonds, insofar as they are well correlated with experimental heats of adsorption. Based on these correlations, and combining adapted Brønsted–Evans–Polanyi free energy relationships and simple Langmuir–Hinshelwood rate expressions, we show that the trends in experimental activity patterns across the periodic table can be explained by a single variable, the relevant bond energy descriptor. We obtain "volcano" curves with strong maxima, at bond energies that indicate optimal chemical properties. Activities of metallic formulations involving binary alloys in hydrogenation and hydrogenolysis reactions, as well as of ternary sulfides in hydrodesulfurization, are correctly predicted by the metal–carbon or metal–sulfur bond energy descriptors calculated for simple structural models. Our approach therefore provides useful exploratory guidelines.

Keywords: Periodic trends in catalysis; Kinetic models; Bond energies; Descriptors; DFT; Hydrogenation; Hydrogenolysis; Hydrodesulfurization; Compensation effect

1. Introduction

The principle of Sabatier [1], in its time a significant step toward a rational understanding of catalysis, states, according to its original formulation, that the maximum rate will be achieved by a catalyst whose combination with reactants is of intermediate stability, to be effectively active while still transient. Today, most authors rephrase this principle in terms of the optimal heterogeneous catalyst providing neither too weak nor too strong interactions of its surface with the reaction partners in the rate determining step (r.d.s) [2]. The principle of Sabatier, however, could not really be applied to an a priori design of new heterogeneous catalysts until now, mainly due to lack of suitable quantitative means for determining interaction strengths. Modern computational material science techniques should contribute to filling this gap between concept and application: the purpose of the present paper is to show how experimental activity patterns can be correlated to computed bond energy descriptors in accordance with the principle of Sabatier.

We have previously shown that the activity pattern of binary bulk sulfides of transition metals for the hydrodesulfurization of dibenzothiophene [3] reveals a "volcano curve" when projected along the axis of the metal–sulfur (M–S) bond energy E_{MS} [4,5]. We have defined E_{MS} as the cohesive energy per metal–sulfur bond in the bulk binary sulfide, i.e., the ratio of the cohesive energy involved in M–S interactions over the number of M–S bonds, assuming bonds formed by a central atom are localized in its first coordination sphere. We now extend the scope of our work to other organic reactions catalyzed by transition metals. For that purpose, we calculated descriptors of the chemical interactions between X = O, C, H, and metals of the three transition series, following an approach similar to that for sulfides, but starting from bulk oxides, carbides, and hydrides. This is possible as long as our original concept can be modified to provide a general way of separating contributions by like and unlike atoms to the cohesive energy. We present here this improved concept, and the extent to which the bond en-

* Corresponding author.
E-mail address: herve.toulhoat@ifp.fr (H. Toulhoat).

0021-9517/03/$ – see front matter
doi:10.1016/S0021-9517(02)00118-5

ergy descriptors (BED) computed for bulk phases pertain to chemisorption at surfaces.

We show further how activity patterns can be modeled on the basis of classical formal kinetics equations, incorporating the variations from one solid to another solely through the BED. According to our analysis, the activity patterns for these reactions transform into "volcano curves" when plotted against the relevant BED, sharply peaking at optimal bond strengths. Finally, we show that "chemical interpolations" or extrapolations are possible, in the sense that the BED calculated for alloys help to correctly predict their catalytic activity. We conclude that our approach opens the way to virtual screening of potential catalytic materials.

2. Theoretical methods

2.1. Calculation of bond energy descriptors

We call our new scheme the "Yin–Yang" method: it consists in computing the total energy per unit cell of the bulk compound M_aX_b, $E(Yin–Yang)$, that of the same unit cell with atoms X removed, $E(Yin)$, and finally that of the same unit cell from which all atoms except X have been removed, $E(Yang)$. Furthermore, we compute the number n of nearest neighbor atoms M to any atom X per unit cell. We define the bond energy descriptor E_{MX} as

$$E_{MX} = \big[-E(Yin–Yang) + E(Yin) + E(Yang)\big]/n. \tag{1}$$

E_{MX} can therefore be viewed as a "rebonding" energy of X to its complement in the original bulk structure MX. Patents have been applied covering the calculation of this descriptor and its usage in a process for designing new materials [6].

All calculations were performed through the MedeA interface [7]. Structures of the relevant hydrides, carbides, oxides, and sulfides were recovered from the Crystmet and ICSD crystallographic databases [8] through the InfomaticA [7] module, which was also helpful in analyzing these structures and providing them as inputs of ab initio calculations.

Total energy calculations were performed with the VASP software [9], within the density functional theory, using spin polarized projected augmented wavefunctions in the generalized gradient approximation, and periodic boundary conditions. The unit cell parameters were optimized in order to minimize the total energy of the bulk system under the approximations made in VASP. Ten irreducible k-points were considered for the NaCl structures and six for the rutile structures. We estimate the maximum absolute error on computed BEDs to be 30 meV ($\sim 3\ \mathrm{kJ\,mol^{-1}}$). As we have already reported in the case of sulfides [5], cohesive energies computed at the DFT level are expected to deviate by less than 10% from experimental values. The linear correlation we obtained for computed (at 0 K) versus experimental standard heats of formation of oxides ΔH_f^0 is remarkable with a linear regression resulting in ΔH_f^0 (computed) $= 0.94\Delta H_f^0$ (experimental), with a coefficient of correlation $\Re^2 = 0.987$. It reveals, however, a systematic underestimation of ΔH_f^0 by 6–7%. Computed lattice parameters were generally found to be within 2% of the available experimental values.

2.2. Kinetic modeling

Our analysis is in the same spirit as that proposed by Kasztelan a decade ago [10]. The work by Golodets [11] on heterogeneous catalytic oxidations, presented concepts of similar but not identical nature.

Let us consider for a given reaction a set $[c_j]$ of heterogeneous catalysts, and assume they all function according to the same activated microscopic mechanism. At steady state, temperature T, and with fixed chemical potentials μ_i of species i (reactants or products) in the fluid phase, differences in reaction rates r_j can be assigned solely to different free energies of activation $\Delta G_j^{\pm}$ and/or coverages θ_{ji} of the active surfaces by adsorbed species. Assuming equilibrium between adsorbed and fluid phases, the coverages can be expressed as functions of T, μ_i, and the free energies of adsorption of reactants and products $\Delta G_{ji}^{\mathrm{ads}}$. Brønsted–Evans–Polanyi linear free energy relationships (BEP-LFER) are written as (see, for instance [2])

$$\Delta G_j^{\pm} = \gamma_p \Delta_r G + \Delta G_0^{\pm}, \tag{2}$$

where $\Delta G_0^{\pm}$ stands for the intrinsic barrier to the reaction, $\Delta_r G$ for the free energy difference of the reaction, and γ_p for the Polanyi reaction coefficient. In the context of heterogeneous catalysis, we are concerned with the origin of rate differences, thus of activation barrier differences, between different catalysts, for the same chemical reaction. The overall change in the free energy of reaction is the same for all the catalysts; thus if a BEP-LFER holds, the relevant $\Delta_r G$ is not the overall change in free energy, but the free energy difference between products and reactants for the rate determining step in the adsorbed state, as proposed earlier [10]. We can write with subscripts p and r particularizing products and reactants in the r.d.s.,

$$\Delta_r G = \sum_p \Delta G_{j,p}^{\mathrm{ads}} - \sum_r \Delta G_{j,r}^{\mathrm{ads}}. \tag{3}$$

Combining (2) and (3), one obtains a LFER relating, $\Delta G_j^{\pm}$ and the $\Delta G_{j,i}^{\mathrm{ads}}$. The final step is to assume linear relationships between the $\Delta G_{j,i}^{\mathrm{ads}}$ and relevant bond energy descriptors E_j, as will be demonstrated empirically in the next section. Hence, a LFER will also relate $\Delta G_j^{\pm}$ and E_j. A particular solid is indexed by the subscript j and an adsorbed species by the subscript i to give

$$\Delta G_j^{\pm} = \alpha E_j + \Delta G_0^{\pm} \tag{4}$$

and referring free energies of adsorption to the standard state

$$\Delta G_{j,i}^{0,\mathrm{ads}} = \beta_i E_j + \Delta G_{0,i}^{0,\mathrm{ads}}. \tag{5}$$

Relationships similar to (4) have recently been obtained by Logadottir et al. [12] on the basis of a DFT study

of N_2 activation on various model surfaces. If the linear Eqs. (4) and (5) hold, we are able in principle to represent the influence of the catalyst in an activity pattern by a single numerical variable, or descriptor, E_j. According to the principle of Sabatier, it was expected to find such a descriptor with the physical meaning of a binding energy between an element of the catalyst and an element of the reactants.

We illustrate further the application of Eqs. (4) and (5) in a particular case, but of broad applicability, a reaction with a Langmuir–Hinshelwood mechanism, involving a bimolecular rate determining step in the adsorbed phase:

$$A_{\text{ads}} + B_{\text{ads}} \rightarrow C_{\text{ads}}. \tag{R1}$$

Reactants and products are assumed to compete for a single type of surface site the total amount of which is fixed. The reaction rate r_j on the catalyst C_j is equal to

$$r_j = \left(\frac{kT}{h}\right) \exp\left(\frac{-\Delta G_j^{\pm}}{RT}\right) \theta_{jA}\theta_{jB}, \tag{6}$$

with k and h the Boltzmann and Planck's constants, respectively. The fractional coverages in A, B, and C are proportional to the fraction of free sites θ_j^* according to the law of mass action

$$\theta_{jA} = P_A \theta_j^* \exp\left(\frac{-\Delta G_{j,A}^{0,\text{ads}}}{RT}\right), \text{ (respectively, } B,\ C) \tag{7}$$

where P_A (respectively, P_B, P_C) is the fugacity of A (respectively, B, C) in the fluid phase, and $\Delta G_{j,A}^{0,\text{ads}}$ is now the standard free energy of adsorption of reactant A over the surface of catalyst j. The balance equation for surface sites gives

$$\theta_{jA} + \theta_{jB} + \theta_{jC} + \theta_j^* = 1. \tag{8}$$

Eliminating fractional coverages in (6) through (7) and (8) leads to

$$r_j = \left(\frac{kT}{h}\right) P_A P_B \exp\left(\frac{-\Delta G_j^{\pm} - \Delta G_{j,A}^{0,\text{ads}} - \Delta G_{j,B}^{0,\text{ads}}}{RT}\right) \times \left[1 + \sum_i P_i \exp\left(\frac{\Delta G_{j,i}^{0,\text{ads}}}{RT}\right)\right]. \tag{9}$$

It is well known that Eq. (9), due to Langmuir, goes through a marked maximum as either θ_{jA} or θ_{jB} span the $\{0, 1\}$ interval. Substituting in (9) for $\Delta G_j^{\pm}$, $\Delta G_{j,A}^{0,\text{ads}}$, $\Delta G_{j,B}^{0,\text{ads}}$, and $\Delta G_{j,C}^{0,\text{ads}}$, by making use of (4) and (5) leads finally to a master rate expression dependent on a set of parameters and variables listed as

$$r_j = r_j\left(E_j, \alpha, \Delta G_0^{\pm}, \beta_A, \beta_B, \beta_C, \Delta G_{0,A}^{0,\text{ads}}, \Delta G_{0,B}^{0,\text{ads}}, \Delta G_{0,C}^{0,\text{ads}}, P_A, P_B, P_C, T\right). \tag{10}$$

In its explicit form, Eq. (10) models an activity pattern with one variable describing the solid catalyst, E_j, variables expressing the operating conditions chosen for the catalytic activity measurements, and a set of constants to be determined.

The central proposal of the present study is that once these constants have been determined for a given reaction, thanks to a set of known *chemically related* catalytic materials for which the descriptors E_j can be computed, it is possible to *predict* the catalytic activity of an untested material u from the sole computation of its descriptor E_u. By *chemically related*, we mean generally the stable form of an association of elements under the prevailing operating conditions: oxides under oxidizing conditions, sulfides under sulfiding conditions, and carbided metallic alloys under reducing conditions.

Notice finally that according to (9) the logarithmic derivative of $r_j(E_j)$, with respect to T^{-1}, will give the apparent energy of activation $E^{\text{app}}(E_j)$, and that the apparent preexponential factor $A(E_j)$ can be defined from $r_j(E_j) = A(E_j)\exp[E^{\text{app}}(E_j)/RT]$.

We have performed many numerical tests showing that within a rather large domain of the parameter space, $\ln A(E_j)$ and $E^{\text{app}}(E_j)$ are linearly correlated, so that the model reproduces the so-called "compensation effect" [13], a feature almost always characteristic of consistent activity patterns. This point will be illustrated in Section 3.3.4 as an example. Patterson and Rooney proposed an explanation of the compensation effect along very different lines some time ago [14].

3. Results and discussion

3.1. Periodic trends for bond energy descriptors

Obviously, the bond energy descriptors will depend on the structure considered. We have calculated E_{MC} for MC carbides in the NaCl structure, where M stands for a transition element of the 3d, 4d, and 5d series. MC carbides are known for most early transition elements (TM), while they are metastable or unstable under usual conditions for late TMs. We have obtained also a good linear correlation between computed (at 0 K) and experimental standard heats of formation of known MC carbides. The linear regression resulted in ΔH_{f}^0 (computed) $= 0.81\ \Delta H_{\text{f}}^0$ (experimental) $- 10$ (in kJ mol^{-1}), with $\Re^2 = 0.92$. For a consistent comparison across the whole transition series, and obviously because they happen to be the most relevant for catalysis, we have included the late TM carbides, although they may exhibit positive standard heats of formation. The periodic trends obtained are presented in Fig. 1: the general tendency is for E_{MC} to decrease continuously for the three series beyond Ti, Zr, and Hf, as the d-band fills and antibonding orbitals become occupied, in conformity with the general analysis recently presented by Hammer and Nørskov [15]. In the NaCl structure, transition-element atoms have only carbon in octahedral symmetry in their

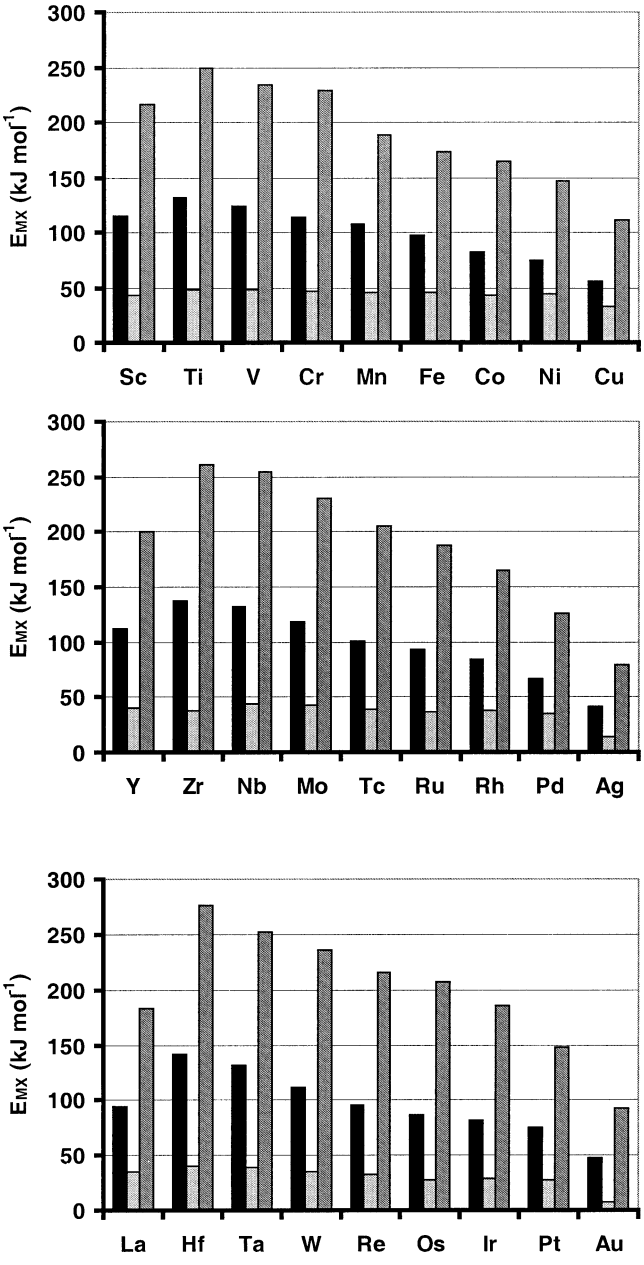

Fig. 1. Periodic trends obtained for the BED E_{MC} computed in the NaCl (Fm-3m) MC carbide structure (black), E_{MH} computed in the NaCl (Fm-3m) MH hydride structure (light gray), and E_{MO} computed in the Rutile (P42/mnm) MO_2 oxide structure (dark gray).

first coordination sphere, a situation resembling that of coordination complexes. Similar but much less marked trends are obtained for E_{MH} computed for hydrides in the same NaCl structure as shown in Fig. 1.

We show in Fig. 1 the rather regular trend obtained for E_{MO} when M is varied in the MO_2 rutile structure, whereas there are marked variations of E_{MO} when the ratio m/n in a M_nO_m structure, hence the degree of oxidation of M varies. Generally, E_{MO} increases as m/n increases; that is, the bond gets stronger as the TM ion is more oxidized. There are exceptions however, such as for copper oxides, where a maximum is found for CuO.

Finally, notice in Fig. 1 that descriptors for the d^1s^2 first elements in each series Sc, Y, and La, exhibit lower values than expected and present an exception to the trend of decreasing bond strengths as the d-band fills. A detailed interpretation of this behavior is, however, beyond the scope of the present paper.

3.2. Correlations of experimental heats of adsorption on metals with bond energy descriptors

In what follows, we have used published data for isosteric initial heats of adsorption of various molecular species on transition metal surfaces [1,3,12]. Most of these values have been obtained some time ago by standard calorimetric techniques, and for dispersed metals rather than well-defined monocrystalline surfaces prepared under ultra high vacuum conditions. Although not suited for testing computational predictions for adsorption on slab models, these data which integrate the presence of corners, kinks, and steps, at the surfaces of small or even nanosized TM particles, are probably rather relevant for actual supported catalysts, on which the vast majority of available activity patterns was measured.

3.2.1. Adsorption of oxygen

A fairly good linear correlation ($\Re^2 = 0.93$) exists between experimental isosteric heats of adsorption of O_2 on metals, $Q_{ads}^{O_2}$, and the theoretical descriptor E_{MO} computed in the rutile structure with a linear regression resulting in

$$Q_{ads}^{O_2} = 4.41E_{MO} - 236 \text{ (in kJ mol}^{-1}\text{)}.$$

We do not find a good correlation of E_{MO}, neither with the quantity q_s introduced by Boreskov et al. [16], as reported by Golodets in [11], nor with the quantity q_O initially proposed by Rethwisch and Dumesic [17] and tabulated by Idriss and Barteau [18]. Since we noticed that q_s and q_O correlate poorly with $Q_{ads}^{O_2}$, we conclude that these quantities assume physical meanings different from that of our BED.

3.2.2. Adsorption of sulfur

Heats of adsorption of sulfur on transition metals are scarce. In a seminal paper, Bénard et al. [19] showed that the heats of formation of "bidimensional" TM sulfides are linearly correlated to those of the corresponding bulk sulfides, implying that metal-sulfur bond strengths are comparable for sulfur adatoms on well-defined TM surfaces and for bulk TMS. Their data can be converted into heats of adsorption of sulfur on metal surfaces by adding the surface energies (or half the cohesive energies) necessary to create these surfaces. The linear correlation with our computed BED E_{MS} is fairly good, with a linear regression resulting in

$$-\Delta H_{S/M} = 3.3E_{MS} + 209 \text{ (in kJ mol}^{-1}\text{)},$$
$$\text{with } \Re^2 = 0.92.$$

The slope close to 3 suggests that chemisorbed sulfur is in general threefold coordinated.

3.2.3. Adsorption of dihydrogen

Following our guideline, we have tried to correlate experimental heats of adsorption of dihydrogen with E_{MH} as computed from various existing hydride structures. Dihydrogen is indeed known to dissociate rapidly on late as well as early TMs [3]. The result was generally quite poor in the case of MH hydrides of NaCl structure. No other structure reported for TM hydrides gave a significantly better correlation. Notice, however, that in the case of hydrides and heats of adsorption of dihydrogen, error bars on experimental as well as computed values are rather large. Surprisingly a fairly good linear correlation was found with E_{MC}, with a linear regression resulting in

$$Q_{ads}^{H_2} = 1.7E_{MC} - 41 \text{ (in kJ mol}^{-1}\text{)}, \quad \text{with } \Re^2 = 0.89.$$

In what follows, we will take this result from an empirical standpoint only, as the development of a theoretical understanding of such a correlation is beyond the scope of the present work.

3.2.4. Adsorption of ethene

We have found that heats of adsorption of ethene on TMs show overall a fairly good linear correlation with E_{MC}, as shown in Fig. 2 ($\Re^2 = 0.92$). A closer look, however, reveals that late TMs are characterized by heats of adsorption clustered around 100 kJ mol^{-1}. In the case of Pt, this value has been assigned to molecularly adsorbed ethene

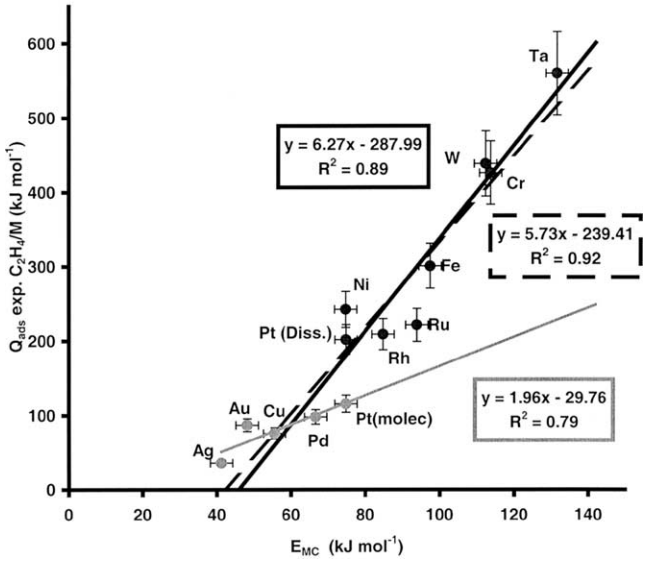

Fig. 2. Correlations between initial heat of adsorption of ethene on TM films [13,22] and the computed BED E_{MC} in the NaCl (Fm-3m) MC carbide structure: The data are divided into two groups, including either the late (●, dissociative) or the early (◍, nondissociative) transition metals with regression lines and equations. Also shown are the regression line (– – –) and regression (discontinuous frame) obtained when the two groups of data are merged.

(di-σ), while the heat is nearly doubled at a higher temperature when the adsorption has become dissociative, leaving two triply coordinated ≡CH fragments on separate threefold hollows of the surface [20]. One can therefore divide the data into two groups, the cluster around 100 kJ mol^{-1} corresponding to late TMs, and the rest. This division is supported by the known evolution with increasing temperature of chemisorbed configurations as reviewed by Yagasaki and Masel [21] and further analyzed by Masel (see discussion in [3, p. 166]): starting from π-bonded or di-σ-bonded ethene on TM close-packed faces at low temperatures, the configuration evolves at higher temperatures through dehydrogenation toward triply bonded (three C–M bonds) ethylidine on group VIII (late) TMs, and toward more strongly bonded acetylene (two C=M double bonds) on earlier TMs (e.g., Ni, Ru, Fe, W, …), to end up as mentioned, with the state in which the molecule is dissociated into two ≡CH fragments. When correlations with E_{MC} are sought separately for the two groups, two least-squares regression lines are obtained as shown also in Fig. 2. We will take as meaningful only the one corresponding to early TMs (with $\Re^2 = 0.89$, slope 6.3, and intercept −290 kJ mol^{-1}) the other showing that essentially no periodic trend emerges for ethene adsorption on late TMs. The slope close to 6 supports the suggestion that under the prevailing experimental conditions, early TMs dissociate an ethene molecule into two CH moieties triply bonded to the surface, thus creating six M–C bonds.

3.3. Kinetic interpretation of experimental periodic trends

Through the previous section, we have been able to exhibit linear relationships such as that expressed by Eq. (5) between enthalpies of adsorption and bond energy descriptors: the linearity holds at least piecewise, and for the time being, we neglect entropic corrections. Below, we build upon these relationships and the analysis developed in Section 2.2 in order to interpret experimental activity patterns known for various important catalytic reactions.

3.3.1. Hydrogenation of ethene

We use the classical activity data from Beeck [22] for metal films obtained by PVD on glass, and those of Schuit and van Reijen [23], for silica-supported metallic particles. All turnover frequencies (TOF) have been renormalized to a reaction temperature of 200 K and $P_{H_2}/P_{C_2H_4} = 1$, using the apparent activation energies and reaction orders found by these authors. The activity patterns are plotted against E_{MC} (from NaCl MC carbides) in Fig. 3, on a semilogarithmic scale. Also shown in Fig. 3 is the theoretical relationship of the type [10] best fitting the data of Schuit and van Reijen. This curve is not a simple volcano, but a "double-peaked" volcano, defining therefore two activity "windows" inside which ethene hydrogenation rates become significant. We have assumed a Langmuir–Hinshelwood rate equation, as presented in Section 2.2, where ethene and

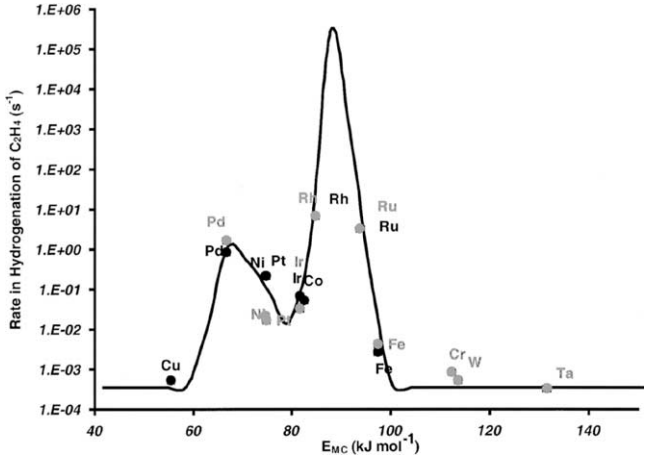

Fig. 3. Pattern of experimental activity (log scale) for the hydrogenation of ethene ([23] ●, [22] ●) plotted against the computed BED E_{MC} in the NaCl (Fm-3m) MC carbide structure. (—): theoretical relationship of type (10) best fitting the data for silica-supported metals [23].

hydrogen compete for the same sites, and the product ethane desorbs as soon as formed. Such a kinetic model has already been shown to fit experimental data for hydrogenation of ethene over silica-supported nickel [24]. Fig. 4 shows the linear relationships of types (4) and (5) of ΔG against E_{MC}, which determine the theoretical profile in Fig. 3. For chemisorption of dihydrogen, we have used exactly the correlation mentioned in Section 3.2.3. For adsorption of ethene, and following the result shown in Fig. 2, we have split the relationship into two parts. The first part with slope 0 (constant enthalpy of adsorption) corresponds to late (or noble) TMs, with $E_{MC} < 79\ \mathrm{kJ\,mol^{-1}}$, and the second part with slope -6 corresponds to early TMs, with higher values of E_{MC}. For the BEP-LFER, also shown in Fig. 4, we have fixed the slope α to -1 and adjusted the

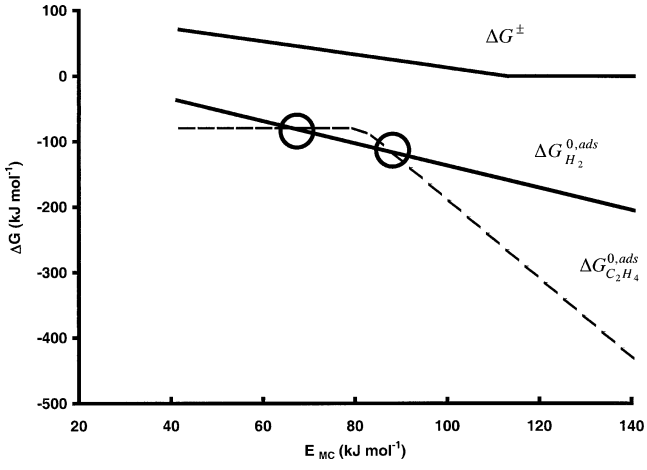

Fig. 4. Linear relationships of types (4) and (5) which determine the theoretical profile for the hydrogenation of ethene in Fig. 3. E_{MC} is computed according to the "Yin–Yang" method in the NaCl (Fm-3m) MC carbide structure at the DFT/GGA/PAW/SP level. Black circles indicate the crossing points which determine the maxima in the theoretical activity profile in Fig. 3

intercept $\Delta G_0^{\pm}$ to optimize the coefficient of correlation of a linear regression of predicted with respect to experimental log(TOF). We achieved $\Re^2 \approx 0.98$, making use of the data of Schuit and van Reijen [23] only. This yields an almost constant apparent activation energy of 50 $\mathrm{kJ\,mol^{-1}}$ in the range 60–100 $\mathrm{kJ\,mol^{-1}}$ for E_{MC}, where significant catalytic activities emerge, a value very close to the experimental data reported by Schuit and van Reijen [23]. The two maxima in the theoretical curve in Fig. 3 correspond to the two circled crossover points in Fig. 4, where the enthalpies of adsorption are equal for both reactants: as partial pressures are equal, coverages in hydrogen and ethene in adsorbed phase are equal for these two particular values of E_{MC} ($E_{MC}^{*1} \approx 66\ \mathrm{kJ\,mol^{-1}}$ and $E_{MC}^{*2} \approx 88\ \mathrm{kJ\,mol^{-1}}$), and local maxima of the LH rate equation are reached.

3.3.2. Hydrogenation of benzene

For this reaction, we have chosen the set of data obtained by Brunelle et al. [25] for γ-alumina supported TMs. The rates are plotted against E_{MC} in Fig. 5, together with the theoretical relationship of type [10] best fitting the data. Here again we have adopted the simplest LH model, assuming that benzene and dihydrogen compete for the same surface sites. As above, no attempt has been made to take into account H_2 dissociation, nor to describe the "site" in terms of an ensemble of surface crystallographic positions. According to recent computational and surface science studies [26], benzene chemisorbs "flat" on well-defined high index TM surfaces, and it is an obvious case of "multipoint" adsorption. The LH model is flexible, however, and in this case "competition" may mean simply that the

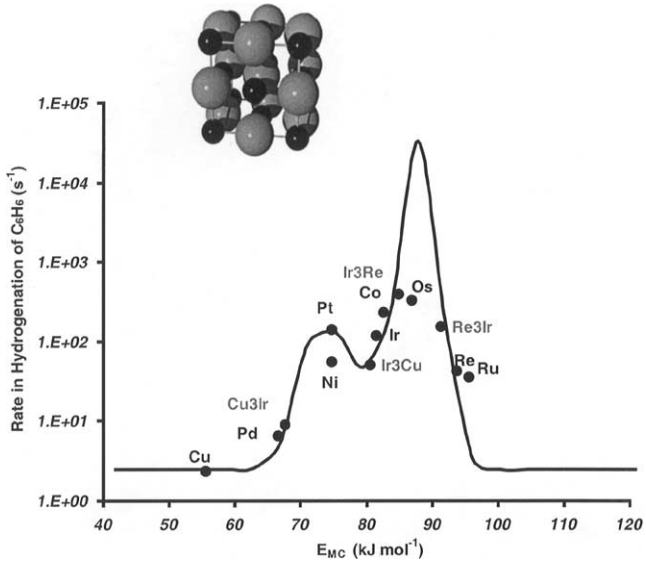

Fig. 5. Pattern of experimental activity (log scale) for the hydrogenation of benzene ([25], ●) plotted against the computed BED E_{MC} in the NaCl (Fm-3m) MC carbide structure. (—): theoretical relationship of type (10) that best fits the data. Experimental data [25] for binary alloys (gray legends) obtained under the same conditions are superimposed. For these alloys E_{MC} is computed in the A_3BC_4 structure as shown in the inset.

adsorption of a single H2 molecule (dissociative or not) might locally prevent the multipoint adsorption of a benzene molecule, and vice versa. The linear relationships of types (4) and (5) which determine the theoretical curve in Fig. 5 are very similar to those presented in Fig. 4. The only differences with the previous case of ethene hydrogenation are: (i) the level of adsorption enthalpy on late TM surfaces has been slightly increased to 90 kJ mol^{-1}, in order to match DFT results for benzene adsorption on high index TM surfaces [27]; (ii) $\Delta G_0^{\pm}$ has been adjusted to obtain the best fit between experimental and theoretical rates (see procedure above, $\Re^2 \approx 0.79$). We still observe two activity maxima, the first, less intense, for late TMs, peaked in the vicinity of Pt, and the second two orders of magnitude higher, approximately 12 kJ mol^{-1} higher on the E_{MC} scale, that is, somewhere between Os and Ru.

3.3.3. Hydrogenolysis of pentane

For the hydrogenolysis of pentane, we have again used the data of Brunelle et al. [25] obtained on the same γ-alumina supported TM catalysts, on which they measured activities in the hydrogenation of benzene. The experimental and theoretical patterns are presented in Fig. 6. We assume pentane adsorption to be negligible for late TM, that is to say below $E_{MC} \approx 60$ kJ mol^{-1}. Moreover, we assume that, above this threshold, one metal-carbon bond is created between each carbon atom and a surface metal atom upon dehydrogenative chemisorption of one pentane molecule, so that the slope of $\Delta G^{0,\text{ads}}_{j,C_5H_{12}}$ versus E_{MC} is set to -5. The volcano is now monomodal, as a single crossing point appears for the heats of adsorption of pentane and dihydrogen, at a value of E_{MC} close to that of osmium.

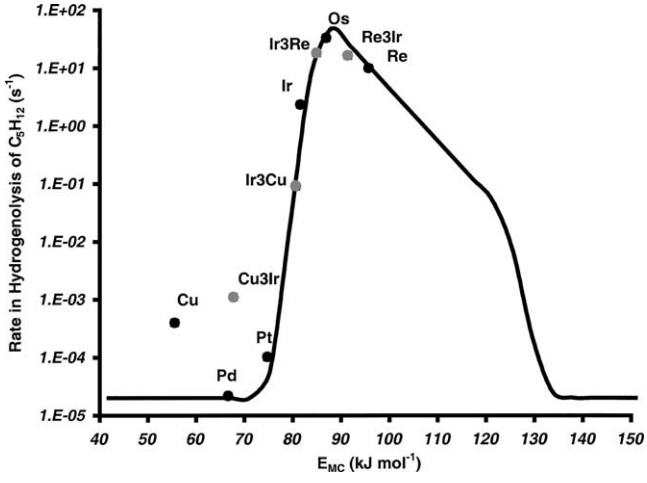

Fig. 6. Pattern of experimental activity (log scale) pattern for the hydrogenolysis of pentane ([25], ●) plotted against the computed BED E_{MC} in the NaCl (Fm-3m) MC carbide structure. —: theoretical relationship of type (10) best fitting the data. Experimental data [25] for binary alloys (gray legends) under the same conditions are superimposed. For these alloys E_{MC} is computed in the A_3BC_4 structure as shown in Fig. 5.

3.3.4. Hydrodesulfurization of dibenzothiophene

This reaction (HDS of DBT) is a relevant model for the desulfurization of diesel fuels carried out in refineries worldwide. It involves H_2 and dibenzothiophene as reactants, and H_2S and hydrocarbons as products, and is performed between 590 and 690 K under H_2 pressures of a few MPa. The high chemical potential of sulfur in the reaction medium under operating conditions maintains all transition elements in a stable combination with sulfur; therefore catalysts for HDS are to be found among transition-metal sulfides (TMS). Pecoraro and Chianelli were the first to systematically establish an activity pattern for TMS in HDS of DBT [3]. As mentioned above, we have already presented a volcano-shaped correlation between these specific activities of TMS and an earlier version of the metal-sulfur BED [4,5]. Using now the E_{MS} values computed according to the Yin–Yang method we improve the correlation as shown in Fig. 7. In that figure, we also show theoretical relationships of type (10) best fitting the data. In this case, we had to refine the kinetic model somewhat, in order to account for (i) the two parallel pathways experimentally established for the reaction [28], DDS for direct desulfurization leading to biphenyl and H_2S through two Csp^2–S bond cleavages, and HYD for prior hydrogenation of an aromatic side ring followed by Csp^3–S bond cleavages, and (ii) the inhibiting effect of the product H_2S.

The model is again of the Langmuir–Hinshelwood type, assuming that all reactants and H_2S compete for the same sites, identified as anionic (sulfur) vacancies at the solid sulfide surfaces, while hydrocarbon products desorb as soon as formed. Another assumption, supported by recent DFT calculations [29] is that DBT adsorbs either in a η^1 configuration ("vertically" through the sulfur), controlling the DDS path and involving one "site", or in a η^6 configuration (aro-

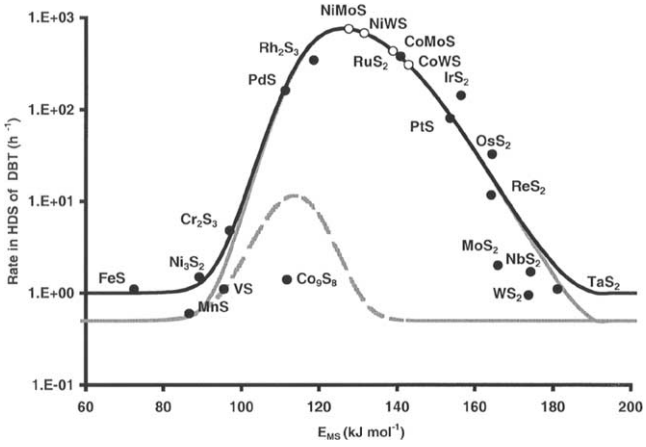

Fig. 7. Pattern of experimental activity (particle size corrected) for the HDS of DBT ([3] ●) plotted against the computed BED E_{MS}. (—): theoretical relationship of the type (10) that best fits the data, sum of the theoretical rates of DDS (—) and of HYD (– –). Predictions for mixed "M′MoS" sulfides (gray legends, ○) are superimposed. The "bulk" averages of E_{MS} computed for binaries are used to locate mixed sulfides, according to the result shown in Fig. 10.

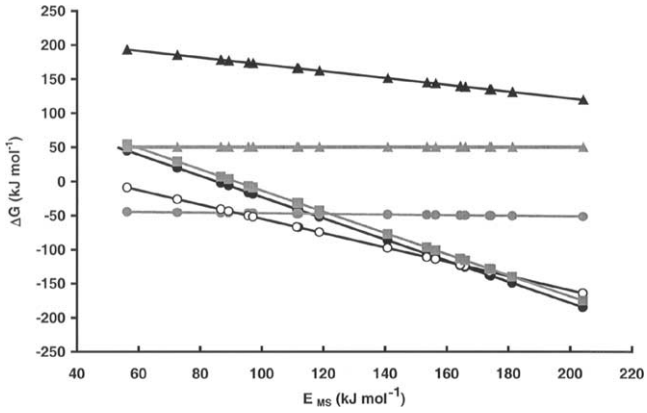

Fig. 8. Linear relationships of types (4) and (5) which determine the theoretical profile for the HDS of DBT in Fig. 7. ●: DBT in η^1; ■: DBT in η^6; ●: H_2; ○: H_2S; ▲: activation energy for the HYD pathway; ▲: activation energy for the DDS pathway.

matic ring "flat" on the solid surface) controlling the HYD path and involving two "sites." The balance equation of type (8) is now quadratic and the positive root in θ_j^* only is retained. The HDS rate for any catalyst is the sum of the DDS and HYD rates, which both take a form analogous to (9) if their rate determining step is the addition of the first H atom to a sp^2 carbon of adsorbed DBT.

We present in Fig. 8 the linear relationships of types (4) and (5) underlying the theoretical curves in Fig. 7. The relationships of type (5) were constrained to match computed heats of adsorption of DBT in η^1 and η^6 modes, H_2 and H_2S, on surfaces sites of both an MoS_2 (10-10) "edge," and a CoMoS model (see top inset of Fig. 10),

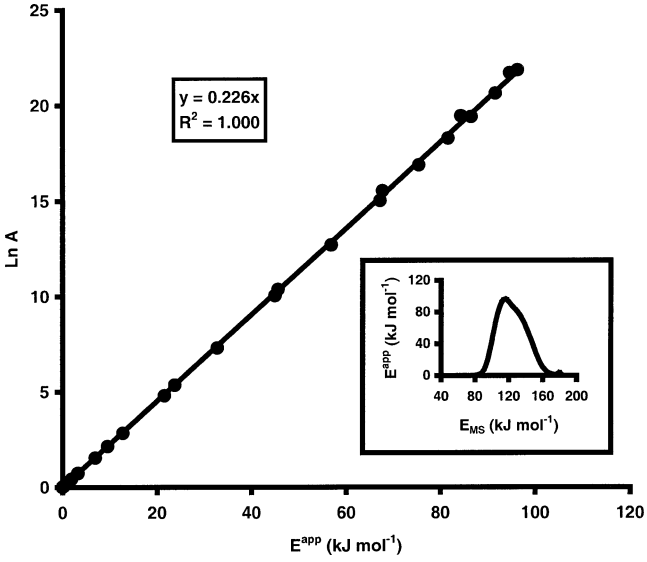

Fig. 9. The compensation effect produced by the kinetic model presented in Fig. 7 for the HDS of DBT. ● correspond to values of E_{MS} varying between 40 and 200 kJ mol^{-1}, by increments of 4 kJ mol^{-1}. $E^{app}(E_{MS})$ is also volcano shaped, and nonzero apparent energies of activation are found only within the "activity" window as shown in the lower inset. The straight line corresponds to a linear least-squares regression with parameters in the upper inset.

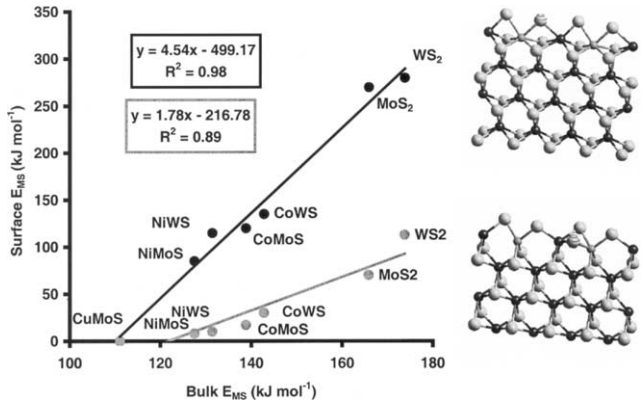

Fig. 10. Linear correlations obtained between surface ("Mo-edge": ●, "S-edge": ●) and bulk E_{MS} and supporting the characterization of nanosized mixed active sulfides by the average of bulk E_{MS} computed for the binaries. Surface E_{MS} is defined as the heat of hydrogenation of a bridging S adatom at a partially decorated edge of MoS_2 or WS_2 and computed at the DFT level (upper inset: "Mo-edge" configurations; lower inset: "S-edge" configurations; S: ●, Mo or W: ●, Co, Ni or Cu: •).

resulting from recent DFT studies [29,30]. The operating conditions are those of the experiments by Pecoraro and Chianelli [3], namely $T = 673$ K, $P_{H_2} = 2.5$ MPa, $P_{DBT} = 0.3$ MPa, and P_{H_2S} being evaluated at 0.04 MPa. The slope and intercept of the BEP-LFERs of type (4) were adjusted for the DDS ($\Delta G_0^{\pm} = 221$ kJ mol^{-1}, $\alpha = -0.5$) and HYD pathways ($\Delta G_0^{\pm} = 50$ kJ mol^{-1}, $\alpha = 0$) to maximize the coefficient of correlation of a linear regression of predicted with respect to experimental log(TOF). Notice that this choice of parameters for the fit corresponds to the best estimate we could achieve with the limited DFT and experimental data available to date. In the future we expect to be able to refine the model on the basis of new experiments and DFT calculations.

As mentioned in Section 2.2, another very interesting feature of our model is that it exhibits the so-called "compensation effect" [13], as shown in Fig. 9. In fact, this property is not particular to the specific description we have chosen for the HDS of DBT, but rather characteristic of Eq. (9), and similar linear relationships hold for the other reactions analyzed in this report.

3.4. Alloying effects: predictions match experiments

We have now to demonstrate that our BED approach can be used to design new catalytic materials for a given reaction, provided the Sabatier "window" has been determined for that reaction. We constructed simple model structures for the ternary "carbides of alloys" with the purpose of reproducing in the half-coordination spheres of carbon the local bonding situation expected to be relevant for carbon sitting at sites of small bimetallic ensembles on the alloy's surface (see inset of Fig. 5 for structure). The descriptors E_{MC} computed for such ternary "carbides of alloys" can be compared to those obtained for binary carbides of the two constituents. They will essentially reflect the chemical pertur-

bation brought about by substituting one metal for another in the proximal coordination spheres of carbon, or in other words the local chemical trends induced by alloying. In as much as bulk trends involving one transition metal appear to be transferable to its surface chemical properties, one expects the same to hold for alloys.

In Figs. 5 and 6, we have superimposed on the volcano plots obtained for pure metals and the reactions considered, the data points corresponding to alloys: the experimental catalytic activities being the ordinates, and the computed descriptors the abscissas. The data points for alloys consistently match the original volcanoes.

Alloys of Cu and Ir exhibit intermediate metal-carbon bond strengths. As a consequence, the activities of these alloys in hydrogenation of benzene (Fig. 5) and hydrogenolysis of pentane (Fig. 6) are found to be intermediate between those of the pure metals. The same is observed for alloys of Ir and Re, but synergetic effects stem in that case from the fact that the pure metals are situated one on the low energy side, the other on the high energy side of the "volcano."

In the case of HDS of DBT by sulfides, we chose to test the prediction of our model against the well-known synergy effect, or in other terms the fact that the association of a 3d TM (Co, Ni), the promoter, and Mo or W in a mixed sulfide isostructural to MoS_2 produces catalysts with specific activities up to two orders of magnitude higher with respect to that of MoS_2 or WS_2 [31–33]. Industrial formulations exclusively involve such synergetic systems. A significant amount of theoretical [34] and experimental [35] results gives strong arguments in favor of the edge substitutional models illustrated in the insets in Fig. 10, which describe the structure of promoted active sites. With such structural models it is possible to use DFT to compute the surface bond strength of a sulfur adatom in bridging position between a promoter and Mo or W. This surface bond strength can be compared to the estimate obtained by averaging between E_{MS} values computed for the corresponding bulk binaries, e.g., Co_9S_8 and MoS_2 for the so-called CoMoS phase. The linear correlations shown in Fig. 10 demonstrate that the averaged E_{MS} indeed describe the adsorptive properties of M′MS active phases with respect to S. It is therefore possible to obtain activities for these synergetic mixed sulfides, predicted according to the theoretical model presented in Fig. 7, when averaged E_{MS} values are used as abscissas: the results are also shown in Fig. 7. Experimental activity measurements were carried out (at 623 K) by Harris and Chianelli on M′MS unsupported mixed ternary sulfides, under similar conditions as those for the reference binaries [36]. Absolute comparisons are difficult because the mixed sulfides were not monophasic, and surfaces areas were relatively low and somewhat different. However, taking MoS_2 as a reference, our theoretical predictions at 623 K match reasonably well the experimental ranking:

Theory:

$$[\mathrm{NiMoS}: 28.2] > [\mathrm{CoMoS}: 16.4] > [\mathrm{MoS_2}: 1]$$

Experiment [36]:

$$[\mathrm{NiMoS}: 7] > [\mathrm{CoMoS}: 4] > [\mathrm{MoS_2}: 1].$$

These examples of predictions of alloying effects covering catalytic reactions carried out with very different materials and under very different operating conditions are not exhaustive of our findings so far. They demonstrate that theoretical chemical bond strength descriptors provide a suitable tool for the prediction of new potentially catalytically active materials.

4. Conclusions

We have presented a new approach to generate ab initio quantitative descriptors of bond strengths in solids. From this, we have obtained new insights into known experimental catalytic activity patterns. Simple kinetic models produce "volcano curves," eventually multimodal, when predicted turnover frequencies are plotted as a function of our chemical descriptors. In general, optimal bond energies can be identified, which describe the best solids, often by orders of magnitude more active than the worst. Moreover, these models reproduce the so-called "compensation effect," which is generally found to characterize experimental activity patterns.

Such models hence provide a unifying quantitative theoretical framework, which can be discussed with respect to the principle of Sabatier, putting forward similarities and differences. Similarly to Sabatier's statement, optimal adsorbate–substrate bond strengths emerge, in that high energy barriers that are too high impede the activation when bond strengths are too weak, and too strong bond strengths poison the surface. The main difference is that the transient intermediate of Sabatier, while retained through the transition state theory formalism, is not sufficient to determine the occurrence of volcanoes in the activity patterns. Rather, the fractional coverage of the catalytic surface by competing reactants is fundamental, because the probability of a reaction, the rate determining step of which is a bimolecular surface reaction, is maximal for equal coverages: this was first described by Balandin [37].

We finally suggest that our theoretical chemical descriptors provide decisive prescreening tools in the context of high throughput and combinatorial exploratory research of new catalysts.

References

[1] P. Sabatier, Berichte der Deutschen Chem. Gesellschaft 44 (1911) 1984.
[2] R.I. Masel, Principles of Adsorption and Reaction on Solid Surfaces, 2nd ed., Wiley, New York, 1996.
[3] T.A. Pecoraro, R.R. Chianelli, J. Catal. 67 (1981) 430.
[4] H. Toulhoat, P. Raybaud, S. Kasztelan, G. Kresse, J. Hafner, Catal. Today 50 (1999) 629–636.

[5] P. Raybaud, G. Kresse, J. Hafner, H. Toulhoat, J. Phys. Condens. Matt. 9 (1997) 11085;
P. Raybaud, G. Kresse, J. Hafner, H. Toulhoat, J. Phys. Condens. Matt. 9 (1997) 11107.
[6] H. Toulhoat, French Patent Application 00/07473, June 9, 2000. US Patent Provisional Application February 28, 2001.
[7] The MedeA suite of modules is marketed by Materials Design s.a.r.l., Le Mans, France.
[8] Crystmet is owned and maintained by Toth Information Systems, Ottawa, and the National Research Council of Canada; ICSD is owned and maintained by the Fach Information Zentrum, Karlsruhe, Germany; both are marketed by Materials Design s.a.r.l., Le Mans, France.
[9] G. Kresse, J. Hafner, J. Phys. Condens. Matt. 6 (1994) 8245;
G. Kresse, J. Hafner, Phys. Rev. B 49 (1994) 14251;
G. Kresse, J. Hafner, Phys. Rev. B 47 (1993) 558;
G. Kresse, J. Fürthmuller, Comput. Mater. Sci. 6 (1996) 15;
The VASP guide is available at http://cms.mpi.univie.ac.at/vasp/.
[10] S. Kasztelan, Appl. Catal. A 83 (1992) L1.
[11] G.I. Golodets, in: Heterogeneous Catalytic Reactions Involving Molecular Oxygen, in: J.R.H. Ross (Ed.), Studies in Surface Science and Catalysis, Vol. 15, Elsevier, Amsterdam, 1983.
[12] A. Logadottir, T.H. Rod, J.K. Nørskov, B. Hammer, S. Dahl, C.J.H. Jacobsen, J. Catal. 197 (2001) 229.
[13] G.C. Bond, Catalysis by Metals, Academic Press, San Diego, CA, 1962.
[14] W.R. Patterson, J.J. Rooney, J. Catal. 146 (1994) 310.
[15] B.V. Hammer, J.K. Nørskov, Adv. Catal. 45 (2000) 71.
[16] G.K. Boreskov, in: Proc. IV Int. Congress on Catalysis, Vol. II, Nauka, Moscow, 1970, p. 437.
[17] D.G. Rethwisch, J.A. Dumesic, Langmuir 2 (1986) 73.
[18] H. Idriss, M.A. Barteau, Adv. Catal. 45 (2000) 261.
[19] J. Bénard, J. Oudard, N. Barbouth, E. Margot, Y. Berthier, Surf. Sci. 88 (1979) L35.
[20] Q. Ge, R. Kose, D.A. King, Adv. Catal. 45 (2000) 207.
[21] E. Yagasaki, R.I. Masel, Catal. Spec. Rep. 111 (1994) 1.
[22] O. Beeck, Rev. Modern Phys. 17 (1945) 61; Disc. Faraday Soc. 8 (1950) 118.
[23] G.C.A. Schuit, L.L. van Reijen, Adv. Catal. 10 (1958) 242.
[24] R. Mezaki, H. Inoue, Rate Equations of Solid-Catalyzed Reactions, University of Tokyo Press, Tokyo, 1991 (cited in Masel [3]).
[25] J.P. Brunelle, R. Montarnal, A. Sugier, C.R.A.S.C 282 (1976) 879;
J.P. Brunelle, R. Montarnal, A. Sugier, in: G.C. Bond (Ed.), Proceedings of the Sixth International Congress on Catalysis Vol. 2, Chem. Society, London, 1977, p. 844.
[26] F. Mittendorfer, PhD thesis, University of Vienna, 2001, references therein.
[27] F. Mittendorfer, P. Raybaud, H. Toulhoat, in preparation.
[28] F. Bataille, J.-L. Lemberton, P. Michaud, G. Perot, M. Vrinat, M. Lemaire, E. Schulz, M. Breysse, S. Kasztelan, J. Catal. 191 (2000) 409.
[29] S. Cristol, J.F. Paul, E. Payen, D. Bougeard, J. Hafner, F. Hutschka, Stud. Surf. Sci. 127 (1999) 327.
[30] P. Raybaud, J. Hafner, G. Kresse, H. Toulhoat, Stud. Surf. Sci. 127 (1999) 309.
[31] H. Topsøe, B.S. Clausen, F.E. Massoth, in: J.R. Anderson, M. Boudard (Eds.), Catalysis, Science and Technology, Vol. 11, Springer, Berlin, 1996.
[32] F.B. Garreau, H. Toulhoat, S. Kasztelan, R. Paulus, Polyhedron 5 (1986) 211.
[33] C. Wivel, R. Candia, B.S. Clausen, S. Mørup, H. Topsøe, J. Catal. 68 (1981) 453.
[34] P. Raybaud, J. Hafner, G. Kresse, S. Kasztelan, H. Toulhoat, J. Catal. 190 (2000) 128;
H. Schweiger, P. Raybaud, H. Toulhoat, J. Catal. 212 (2002) 33.
[35] J.V. Lauritsen, S. Helveg, E. Lægsgaard, I. Stensgaard, B.S. Clausen, H. Topsøe, F. Besenbacher, J. Catal. 197 (2001) 1.
[36] S. Harris, R.R. Chianelli, J. Catal. 98 (1986) 17.
[37] A.A. Balandin, Adv. Catal. 10 (1958) 96.